Glial-conditional deletion of aquaporin-4 (*Aqp4*) reduces blood–brain water uptake and confers barrier function on perivascular astrocyte endfeet

Nadia Nabil Haj-Yasein[a,b], Gry Fluge Vindedal[a], Martine Eilert-Olsen[a,b], Georg Andreas Gundersen[a,b], Øivind Skare[c], Petter Laake[d], Arne Klungland[e], Anna Elisabeth Thorén[a,b], John Michael Burkhardt[a], Ole Petter Ottersen[b], and Erlend Arnulf Nagelhus[a,b,f,1]

[a]Centre for Molecular Medicine Norway, Nordic EMBL Partnership, University of Oslo, 0318 Oslo, Norway; [b]Centre for Molecular Biology and Neuroscience, Letten Centre, Institute of Basic Medical Sciences, University of Oslo, 0317 Oslo, Norway; [c]Division of Epidemiology, Norwegian Institute of Public Health, 0403 Oslo, Norway; [d]Institute of Basic Medical Sciences, Department of Biostatistics, University of Oslo, 0317 Oslo, Norway; [e]Centre for Molecular Biology and Neuroscience, Institute of Medical Microbiology, Oslo University Hospital, 0027 Oslo, Norway; and [f]Department of Neurology, Oslo University Hospital, 0027 Oslo, Norway

Edited by Peter Agre, Johns Hopkins Malaria Research Institute, Baltimore, MD, and approved September 22, 2011 (received for review July 11, 2011)

Tissue- and cell-specific deletion of the *Aqp4* gene is required to differentiate between the numerous pools of aquaporin-4 (AQP4) water channels. A glial-conditional *Aqp4* knockout mouse line was generated to resolve whether astroglial AQP4 controls water exchange across the blood–brain interface. The conditional knockout was driven by the glial fibrillary acidic protein promoter. Brains from conditional *Aqp4* knockouts were devoid of AQP4 as assessed by Western blots, ruling out the presence of a significant endothelial pool of AQP4. In agreement, immunofluorescence analysis of cryostate sections and quantitative immunogold analysis of ultrathin sections revealed no AQP4 signals in capillary endothelia. Compared with litter controls, glial-conditional *Aqp4* knockout mice showed a 31% reduction in brain water uptake after systemic hypoosmotic stress and a delayed postnatal resorption of brain water. Deletion of astroglial *Aqp4* did not affect the barrier function to macromolecules. Our data suggest that the blood–brain barrier (BBB) is more complex than anticipated. Notably, under certain conditions, the astrocyte covering of brain microvessels is rate limiting to water movement.

edema | electron microscopy | homeostasis | membrane | swelling

More than 100 y have elapsed since it was first shown that some solutes present in blood are retained by brain capillaries, pointing to the existence of a barrier function at the blood–brain interface. This early finding naturally inspired a discussion as to what could constitute the morphological substrate of this barrier (1). With the advent of the electron microscope it became clear that the blood–brain interface is composed of endothelia and pericytes, surrounded by a basal lamina and perivascular endfeet of astrocytes. After decades of intense debate, a concept emerged that the functional barrier resides at the level of the endothelial cells (2). This was consistent with morphological data, which clearly showed that endothelia were continuous and coupled by tight junctions (3). The perivascular endfeet, on the other hand, were not coupled by tight junctions and were portrayed as a discontinuous layer with spacious clefts separating the individual processes.

Discussions on the morphological substrate of barrier function have been focused on solutes (4), and the field has not yet matured to provide a consistent view regarding what cellular structures, if any, restrict water movement between blood and brain. Following the discovery of water channels, it became clear that the major brain water channel AQP4 is implicated in water transport at the blood–brain interface. Thus, global *Aqp4* knockout significantly limited the development of brain edema, attesting to the importance of AQP4 water channels (4). As AQP4 is strongly expressed in the perivascular endfeet (5), the interest in these processes was rekindled also in the context of their possible barrier function. Specifically, it was proposed that the endfeet could restrict water flow, most significantly in pathophysiological settings characterized by large water fluxes from blood to brain (6, 7). This conclusion was tempered by the controversy surrounding the exact distribution of AQP4 at the blood–brain interface. Notably, some data indicated that AQP4 was also present in endothelia (8–10). An endothelial pool of AQP4, if any, would have been eliminated after global *Aqp4* deletion and could have accounted for the reduced water absorption and edema formation in $Aqp4^{-/-}$ animals. Global *Aqp4* deletion would also target extracerebral AQP4 pools in kidney and other organs, introducing an experimental confound.

Here we set out to resolve whether the astrocytic pool of AQP4 regulates water flux across the blood–brain barrier (BBB). To this end we used a conditional *Aqp4* knockout strategy where *Aqp4* deletion was driven by the glial fibrillary acidic protein (*GFAP*) promoter. This promoter is expressed in glia but not in endothelial cells (11). By use of the conditional as well as a constitutive *Aqp4* knockout mouse line, we also aimed to resolve the controversy regarding AQP4 expression in endothelial cells. We conclude that endothelial cells are devoid of a detectable AQP4 pool and that the astrocytic pool of AQP4 indeed controls water flux at the blood–brain interface. Thus, when depleted of AQP4, astrocytes restrict water uptake in brain and acquire a barrier function.

Our data are consistent with recent findings showing that the perivascular endfeet constitute a continuous sheath with only narrow spaces between them (12). The present findings imply that any drugs engineered to target AQP4 for therapeutic purposes will have to be designed to permeate the endothelial cell layer.

Results

Effect of Glial-Conditional *Aqp4* Gene Deletion on Brain AQP4 Expression. We used the *GFAP* promoter to target *Aqp4* deletion in glia (Fig. 1*A*). The knockout strategy was successful as AQP4-probed immunoblots of brain homogenates revealed ~32 kDa and 34 kDa bands in controls (flox/flox, f/f), but not in the glial-conditional *Aqp4* knockout (c$Aqp4^{-/-}$) mice (Fig. 1*B*). The blots of c$Aqp4^{-/-}$ mice were indistinguishable from those of constitutive *Aqp4* knockouts, lending no support for AQP4 expression in brain cells other than those expressing the *GFAP* promoter (Fig. 1*B*).

Author contributions: N.N.H.-Y., G.F.V., M.E.-O., G.A.G., A.K., A.E.T., J.M.B., O.P.O., and E.A.N. designed research; N.N.H.-Y., G.F.V., M.E.-O., G.A.G., A.E.T., J.M.B., and E.A.N. performed research; G.F.V., Ø.S., P.L., J.M.B., and E.A.N. analyzed data; and J.M.B., O.P.O., and E.A.N. wrote the paper.

The authors declare no conflict of interest.

This article is a PNAS Direct Submission.

Freely available online through the PNAS open access option.

[1]To whom correspondence should be addressed. E-mail: e.a.nagelhus@ncmm.uio.no.

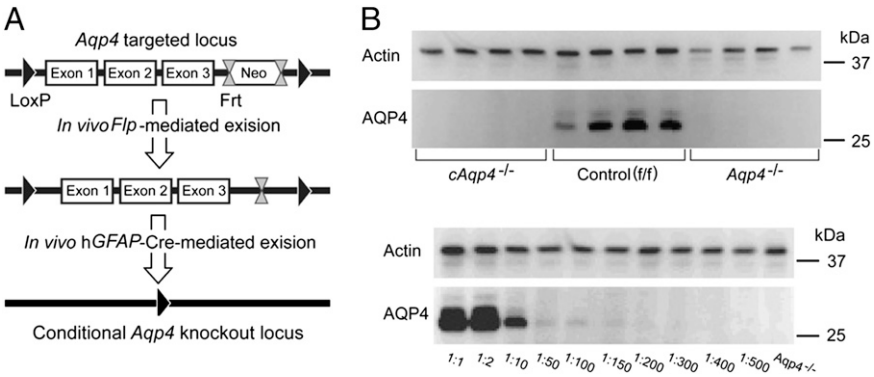

Fig. 1. Strategy for generation and validation of glial-conditional *Aqp4* knockout mice. (*A*) FRT-neomycin-FRT-LoxP validated cassette was inserted downstream of exon (Ex) 3, and a LoxP site was inserted upstream of exon 1. The Neo cassette was deleted by breeding chimeras with Flp recombinase-expressing mice. Heterozygous *Aqp4* floxed mice were bred with mice expressing Cre recombinase under the human glial fibrillary acidic protein (h*GFAP*) promoter, and after intercrossing offspring, conditional $Aqp4^{-/-}$ ($cAqp4^{-/-}$) mice were obtained. (*B*, *Upper*) Immunoblots of brain homogenates obtained from four $cAqp4^{-/-}$ mice (lanes 1–4), four litter f/f control mice (lanes 5–8), and four constitutive $Aqp4^{-/-}$mice (lanes 9–12). The blots were probed with anti-actin (for loading control) and anti-AQP4 antibodies, as indicated to the *Left*. The AQP4 blot showed two confluent bands of ~32 kDa and 34 kDa in homogenates from f/f control mice. These bands were absent in homogenates from both glial-conditional and constitutive $Aqp4^{-/-}$mice, which were indistinguishable. (*Lower*) Immunoblots of WT brain homogenates diluted in homogenates from constitutive $Aqp4^{-/-}$mice. The blots were probed with antibodies against actin and AQP4, respectively, and show that AQP4 immunosignals easily could be detected when 1% or more of the homogenate originated from WT mice. Actin staining verifies similar loading. The 25-kDa and 37-kDa markers are indicated on the *Right*.

The sensitivity of AQP4 signal detection in our Western blot assay was tested in dilution series where WT brain homogenates had been diluted in homogenates from constitutive $Aqp4^{-/-}$ mice (Fig. 1*B*). We found that AQP4 immunosignals easily could be detected when 1% or more of the homogenate originated from WT mice. As no signal was found in brain tissue of conditional knockout animals, the residual AQP4 pool, if any, must be minute.

In line with earlier reports, WT mice showed distinct AQP4 immunofluorescence around cortical microvessels (Fig. 2*A*). *Aqp4* floxed controls (f/f) were indistinguishable from WT mice in regard to pattern of AQP4 labeling (compare Fig. 2 *A* with *B*). Conditional deletion of *Aqp4* abolished AQP4 immunoreactivity in brain (including ependymocytes), but had no effect on the AQP4 pools of muscle or kidney (compare Fig. 2 *B–E* with *G–J*).

High-power microscopy of brain microvessels in WT and f/f mice revealed strong AQP4 labeling peripheral to CD31 positive endothelial cells, consistent with presence of AQP4 in perivascular astrocytic endfeet (Fig. 2 *K* and *L*). The labeling of endfeet was abolished in $cAqp4^{-/-}$ as well as in $Aqp4^{-/-}$ animals (Fig. 2 *M* and *N*). There was no evidence of any residual AQP4 labeling after glial-conditional *Aqp4* knockout.

High-resolution immunogold cytochemistry showed that gold particles signaling AQP4 were present on perivascular astrocyte endfeet of WT and f/f mice, but not of $Aqp4^{-/-}$ or $cAqp4^{-/-}$ mice (Fig. 3 *A*, *B*, *F*, and *G*). This was confirmed by quantitative immunogold analysis (Fig. 3 *C* and *H*). In addition to the immunogold signal associated with the endfoot membrane, we detected a second and weaker signal overlying the abluminal endothelial cell membrane (Fig. 3 *C* and *H*). Both signals were abolished in the conditional and constitutive *Aqp4* knockout animals. The data indicate that the gold particles over the abluminal endothelial cell membrane reflect antibody binding to aquaporins in adjacent endfoot membranes. In agreement, the abluminal membrane failed to associate with notable immunogold labeling when apposed to pericytes rather than endfoot membranes (Fig. 3*C*).

We next analyzed the gold particle distribution along an axis perpendicular to the endfoot and endothelial membranes. This analysis revealed a single peak that coincided precisely with the astrocytic endfoot membrane (Fig. 3 *D* and *I*). The tail of the gold particle distribution extended to the abluminal endothelial membrane, accounting for the gold particle count associated with this membrane domain. The cross-contamination between the two membranes was clearly demonstrated when the distribution of particles was analyzed with respect to the abluminal endothelial cell membrane. The peak was then skewed in the peripheral direction, by a distance corresponding to the width of the basal lamina (37.6 ± 0.9 nm, $n = 176$, 4 mice; Fig. 3 *E* and *J*). These data substantiate the conclusion that the immunosignal at the blood–brain interface is derived in full from the AQP4 pool in the astrocytic endfoot membrane.

Having concluded that the AQP4 pool at the blood–brain interface is restricted to the endfoot membranes, we asked whether specific deletion of this pool reduces brain water uptake under hypoosmotic stress. The data show that deletion of this pool of AQP4 indeed reduces water accumulation, as recorded 40 min after i.p. water loading (Fig. 4*A*). Compared with litter f/f controls, glial-conditional *Aqp4* knockout mice showed a 31% reduction in brain water uptake (increases in brain water content were $1.40 \pm 0.19\%$ and $0.96 \pm 0.08\%$, respectively).

As shown in Fig. 4*B*, brains from the knockout animals exhibited slightly higher basal water content than brains from f/f control mice. The increased brain water content in $cAqp4^{-/-}$ animals could reflect a prenatal developmental abnormality or a reduced elimination of water in the postnatal phase. To discriminate between these two possibilities we analyzed brain water content at different postnatal stages. The difference between f/f and $cAqp4^{-/-}$ animals first appeared at postnatal day 15 (P15) and was manifest at P28 and P70 (Fig. 4*E*). These data suggest that elimination of glial AQP4 delays water resorption in early postnatal life. Brain mass did not differ significantly between $cAqp4^{-/-}$ animals and f/f controls (Fig. 4*C*).

The finding of increased water content in $cAqp4^{-/-}$ mice was reproduced when measurements were made of the brainstem or individual hemispheres (Fig. 4*D*) in lieu of the whole brain.

To assess the integrity of the blood–brain barrier, we measured the amount of Evans blue retained in brain after systemic injections of this dye. No difference was found between $cAqp4^{-/-}$ and f/f mice (Fig. 4*F*).

Discussion

AQP4 is the predominant aquaporin in brain but is also expressed in a number of other organs, including kidney and striated muscle (6). Previous studies of the physiological and pathophysiological roles of AQP4 in brain have been based on

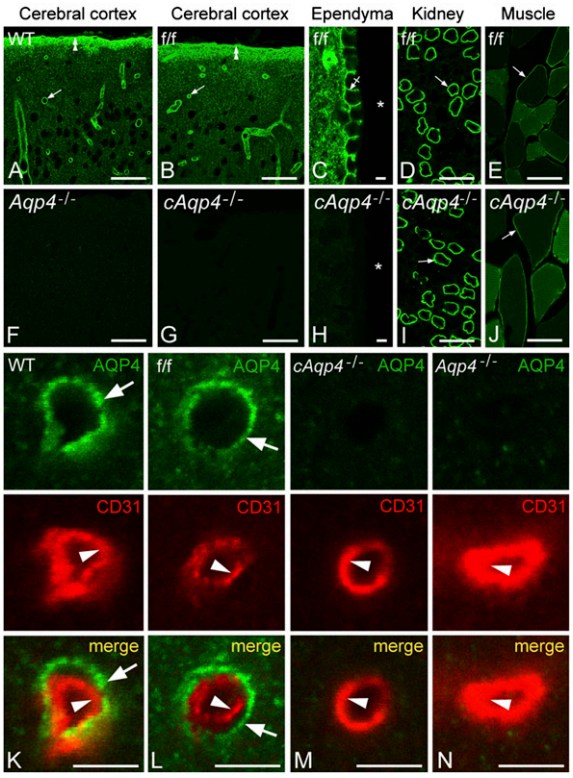

Fig. 2. Immunofluorescence micrographs showing distribution of AQP4. The AQP4 labeling (green) pattern in cerebrum of WT (*A*) and f/f mice (*B* and *C*) was indistinguishable. Note distinct immunosignal around vessels (arrows), underneath the pia (double arrowheads), and along the basolateral membrane of ependymocytes (crossed arrow). Asterisks, third ventricle. In cerebrum of constitutive (*F*) and $cAqp4^{-/-}$ (*G* and *H*) mice, AQP4 immunoreactivity was absent. Conditional deletion of *Aqp4*, however, did not affect the labeling pattern in muscle and kidney (compare *I* and *J* with *D* and *F*; arrows indicate kidney collecting duct and sarcolemma, respectively). Double labeling of obliquely cut capillaries with the endothelial marker CD31 (red) revealed that the AQP4 labeling (green) associated with microvessels in WT and f/f mice was peripheral to the endothelium (arrowhead), corresponding to perivascular astrocytic endfeet (arrows; *K* and *L*). No detectable signal was seen over endothelial cells in either genotype (*K* and *N*). (Scale bars: *A*, *B*, *D*, *E*, *F*, *G*, *I*, and *J*, 50 μm; *C*, *H*, and *K*–*N*, 5 μm.)

analyses of constitutive *Aqp4* knockout animals (7), implying that interpretations might have been confounded by the elimination of extracerebral AQP4 pools. Moreover, some studies have pointed to the possible presence of an endothelial pool of AQP4 in brain (8–10). This would be missing in constitutive knockout animals along with the endfoot pool, complicating the analysis of water transport at the blood–brain interface.

The generation of conditional knockout animals permits specific analyses of the glial pool of AQP4. Thus, the knockout was designed so as to eliminate AQP4 specifically in those cells that express the *GFAP* promoter, i.e., astrocytes, ependymocytes, and oligodendrocytes (11). AQP4-expressing cells in other organs do not express *GFAP* and thus retained their complement of AQP4 after glial-conditional knockout.

Conditional knockout animals lost the immunogold signal over endothelial cell membranes, despite the fact that endothelial cells do not express the *GFAP* promoter (11). We interpret this finding to suggest that the immunogold signal over endothelium [as recorded in the present study and in that of Amiry-Moghaddam et al. (8)] represents antibody binding to AQP4 molecules embedded in the endfoot membrane. The endfoot membrane and abluminal endothelial cell membrane are separated by a basal lamina whose width is comparable to the length of the antibody bridge between epitope and gold particle (13). This means that a fraction of the gold particles signaling endfoot AQP4 will end up close to the abluminal endothelial membrane and be assigned to the latter, as a consequence of the sampling procedure. Thus, in agreement with standard practice (14) all particles located within 23.5 nm of the midpoint of the endothelial membrane were arbitrarily assigned to this.

Additional data support the idea that AQP4 is selectively expressed in endfoot membranes and not in other membranes at the blood–brain interface. First, in WT animals, abluminal endothelial membranes were associated with gold particles only when apposed to endfoot membranes and not when apposed to pericytes (which are devoid of AQP4). Second, when in WT animals the perpendicular distribution of gold particles was analyzed with the abluminal endothelial membrane as reference, the peak immunogold signal coincided precisely with the endfoot membrane. There was no indication of a smaller peak overlying the endothelial membrane. The immunoblots were in agreement, as no detectable signal remained in brain extracts derived from glial-conditional knockout animals. In line with our data, cultured brain microvessel endothelial cells failed to express AQP4 mRNA (15).

The conclusion at this point is that our experimental paradigm allows for a specific analysis of the role of the endfoot pool of AQP4 at the blood–brain interface. In this sense the conditional knockout served a dual purpose: It allowed for the selective depletion of the latter pool and also helped establish that the endfoot pool is the only AQP4 pool that can be conceived to control water flux between blood and brain.

We were now in a position to resolve whether the endfeet can serve to limit water influx in brain. When loaded with water i.p., the glial-conditional *Aqp4* knockout animals showed less water accumulation in brain than f/f animals. This is not due to reduced capacity for water uptake, as brain mass (and, by inference, the potential for brain expansion within the cranial cavity) did not differ between genotypes. Our data indeed suggest that the endfoot AQP4 pool regulates water uptake in pathophysiological conditions. In other words, astrocytes may acquire barrier function and restrict water exchange between brain and blood, dependent on their complement of AQP4. This finding has direct implications for a number of experimental and clinical conditions that are characterized by a loss of perivascular AQP4, including mesial temporal lobe epilepsy (16), experimental stroke (17), and a model of Alzheimer's disease (18).

Given that AQP4 allows bidirectional water transport (6), a second question is whether the endfoot pool of AQP4 plays a role in the resorption of brain water that occurs postnatally (19). Notably, the extracellular volume fraction is highest in the newborn and diminishes with age (20). The developmental analysis clearly showed that water resorption was delayed in the conditional animals compared with WT controls. Interestingly, brain AQP4 expression becomes evident in the second postnatal week (21), at the time when there is a dramatic reduction in extracellular volume fraction (20). The differences in baseline water contents between glial-conditional knockout animals and controls were reproduced in specimens consisting of isolated hemispheres or caudal brainstem. These specimens are drained of ventricular CSF. Thus, the increased brain water content must reflect excess water in brain parenchyma rather than any difference in ventricular volume. If glial-conditional $Aqp4^{-/-}$ animals show an increase in baseline extracellular space volume similar to that reported for constitutive $Aqp4^{-/-}$ (22, 23), this would explain the excess water content.

Having shown that manipulations of the endfoot pool of AQP4 affect brain water uptake and possibly also brain water resorption, we asked whether the deletion of this pool also affects the barrier function to macromolecular compounds. This could occur if loss of AQP4 from endfoot membranes translated

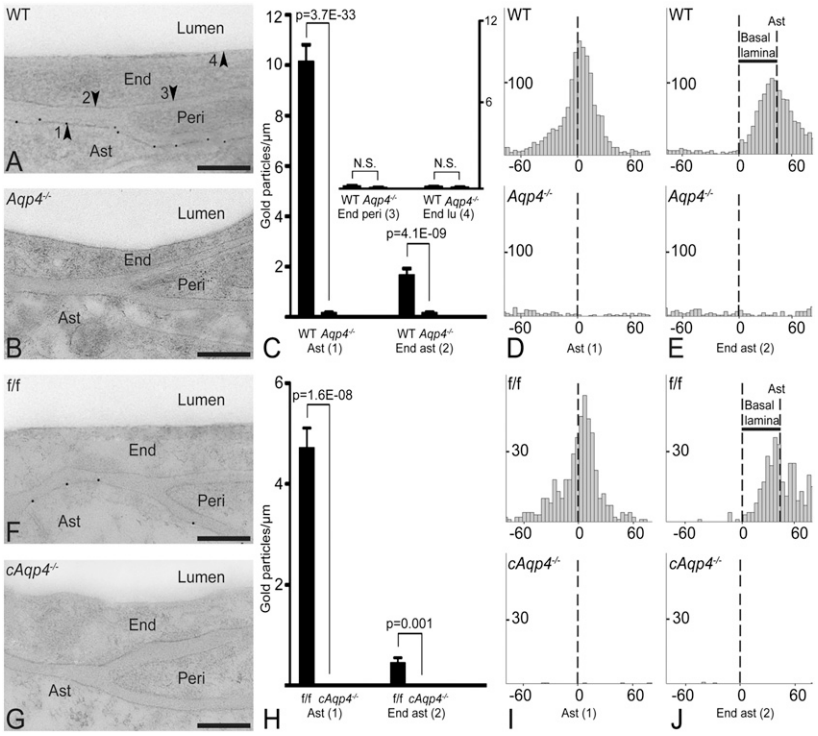

Fig. 3. Subcellular distribution of AQP4 immunogold reactivity. (*A*) Electron micrograph from WT mouse showing AQP4 immunogold particles along the astrocyte (Ast) endfoot membrane. End, endothelial cell; Peri, pericyte. Arrowheads indicate astrocyte endfoot membrane (*1*) and the endothelial membranes facing astrocyte (*2*), pericyte (*3*), and lumen (*4*). (*B*) AQP4 labeling was absent in constitutive *Aqp4* knockout mice ($Aqp4^{-/-}$ mice). (*C*) Quantitative analysis of the density of gold particles over the membrane domains indicated in *A*. The same symbols (*1–4*) are used for easy reference. Gold particles within 23.5 nm from a given membrane were allocated to that membrane. The AQP4 signal over the Ast endfoot membrane was significantly higher in WT than in $Aqp4^{-/-}$ mice. The two genotypes did not differ in AQP4 densities over endothelial membranes facing pericytes (End peri) and lumen (End lu), indicating absence of AQP4 in these membrane domains. The AQP4 signal over endothelial membranes next to astrocyte endfeet (End ast) was higher in WT than in $Aqp4^{-/-}$ mice. (*D* and *E*, *Upper*) Analysis in WT animals of the distribution of gold particles perpendicular to the astrocyte endfoot membrane (Ast, *D*) or to the endothelial membrane facing astrocytes (End ast, *E*) revealed peak immunogold signal coinciding with former membrane. When analysis was performed with abluminal endothelial membrane as reference (*E*) the peak was skewed corresponding to the thickness of the basal lamina (indicated with bar; *Results*). (*D* and *E*, *Lower*) No peaks were seen in $Aqp4^{-/-}$ mice. (*F*) AQP4 immunogold labeling pattern in controls (f/f) was similar to that of WT mice (*A*). (*G*) AQP4 immunoreactivity was absent in glial-conditional *Aqp4* knockout mice ($cAqp4^{-/-}$ mice). (*H*) The linear densities of AQP4 signaling gold particles over astrocytic and apposed endothelial membranes showed a pronounced reduction in $cAqp4^{-/-}$ vs. litter controls (f/f). (*I* and *J*) Same design as in *D* and *E*, respectively, but f/f controls in lieu of WT and $cAqp4^{-/-}$ mice in lieu of $Aqp4^{-/-}$ mice. Perpendicular distribution of gold particles showed absence of peaks after glial-conditional deletion of *Aqp4,* confirming that the immunosignals seen in f/f mice reside in glia. (Scale bars: *A*, *B*, *F*, and *G*, 200 nm.)

into a disruption of tight junctions in the adjacent endothelial membranes. No evidence was found of such a mechanism, as extravasation of Evans blue did not differ between genotypes. Our data on Evans blue extravasation are in line with those reported for constitutive $Aqp4^{-/-}$ mice (24).

Conclusion

The present conditional knockout strategy allowed specific analysis of the glial pool of AQP4, unconfounded by extracerebral pools of this water channel. This strategy also permitted us to conclude that AQP4 expression in brain is restricted to *GFAP* promoter expressing cells and cells derived from them. Most significantly, the conditional knockout animals failed to exhibit any residual immunocytochemical or Western signal for AQP4 in capillary endothelial cells, resolving the controversy surrounding endothelial expression of AQP4. Our data suggest that the perivascular glial covering can limit the rate of brain water influx as well as efflux, despite the fact that this covering is not part of the BBB as traditionally defined.

Materials and Methods

Animals. The generation of glial-conditional *Aqp4* knockout mice was done in collaboration with GenOway (Lyon, France). A FRT-neomycin-FRT-LoxP validated cassette was inserted downstream of exon 3, and a LoxP site was inserted upstream of exon 1. Following homologous recombination in ES cell, ES cell injection into blastocytes, and generation of chimeras, the Neo cassette was deleted by breeding chimeras with Flp recombinase-expressing C57BL/6J mice. Heterozygous floxed mice were bred with Friend leukemia virus B mice expressing Cre recombinase under the human glial fibrillary acidic protein promoter (*GFAP*; stock no. 004600; The Jackson Laboratory). Offspring were subsequently bred with each other to generate Cre^{+} $Aqp4^{flox/flox}$ (glial-conditional $Aqp4^{-/-}$, "$cAqp4^{-/-}$"), Cre^{-} $Aqp4^{flox/flox}$ controls (termed "f/f"), and $Aqp4^{wt/wt}$ (WT). We also used constitutive $Aqp4^{-/-}$ animals, where the knockout allele had been backcrossed in C57BL/6J for five generations (25). Studies were conducted with mice aged 8–18 wk, weighing 20–30 g. The animals were allowed free access to food and drinking water. All experiments were approved by the institution's animal care and use committee.

Western Blotting. After homogenization and solubilization, extracts of mouse brain (sample with 10 μg protein) were loaded onto a 12.5% self-cast SDS/PAGE gel and subsequently transferred onto polyvinylidene difluoride (PVDF) membrane (Bio-Rad), as described previously (14). For the titration series, wild-type homogenate was diluted in constitutive $Aqp4^{-/-}$ sample in set concentrations (Fig. 1*B*) to determine the sensitivity of the immunoblotting. The membrane was probed with goat anti-AQP4 antibody (Santa Cruz; sc-9888; 0.2 μg/mL) followed by alkaline phosphatase-conjugated rabbit antigoat IgG (1:10,000; Sigma), then developed by using the ECF fluorescent substrate (GE Healthcare) and visualized on a Typhoon 9410 scanner (Amersham). The membranes were stripped and reprobed with mouse anti–β-actin (Abcam; ab-8226; 1:500) for loading control.

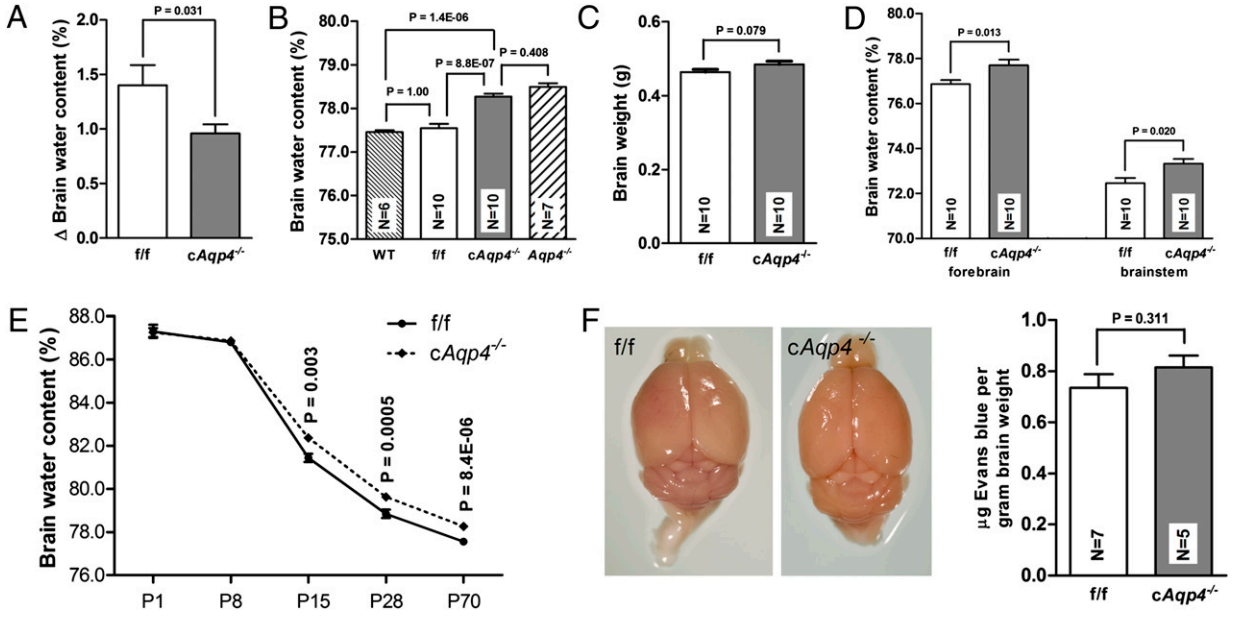

Fig. 4. Effect of glial-conditional *Aqp4* deletion on brain water content and blood–brain barrier permeability. (*A*) Increase in brain water content 40 min after i.p. water injection (150 mL/kg) was significantly lower in *cAqp4*$^{-/-}$ mice than in f/f litter controls. Error bars indicate SE. (*B*) Basal brain water content of *cAqp4*$^{-/-}$ mice was significantly higher than that of WT and f/f controls, but did not differ from that of constitutive *Aqp4*$^{-/-}$ mice. (*C*) Brain mass did not differ significantly between genotypes ($P > 0.05$). (*D*) Baseline water content of forebrain hemispheres and brainstem was higher in *cAQP4*$^{-/-}$ mice than in controls. (*E*) Baseline brain water content at various stages of postnatal development. At postnatal days 1 (P1) and 8 (P8) the genotypes did not differ. At P15, P28, and P70, the brain water content of *cAqp4*$^{-/-}$ mice was significantly higher than that of f/f mice. (*F*) Blood–brain barrier macromolecule permeability. Evans blue staining was not observed in f/f or *cAqp4*$^{-/-}$ mouse brains subsequent to i.v. injection. No significant difference was observed in mean Evans blue content between the two genotypes.

Immunocytochemistry. For all fixation protocols, the animals were deeply anesthetized by an i.p. injection of a mixture of chloral hydrate, magnesium sulfate, and pentobarbital (142, 70, and 32 mg/kg body weight, respectively; Ullevål Sykehusapotek) before transcardiac perfusion with 4% formaldehyde in 0.1 M phosphate buffer (PB) pH 7.4; for immunofluorescence or 4% formaldehyde in PB containing 0.2% picric acid at pH 6.0, followed by a similar fixative at pH 10.0 (for electron microscopic immunocytochemistry) (14).

Light microscopic immunocytochemistry. Light microscopic immunocytochemistry was carried out using a method of indirect fluorescence, as described previously (14). The concentrations of antibodies were: anti-AQP4 (Millipore) 2 μg/mL; anti-rat CD31 (BD Biosciences), 2.5 μg/mL. Cortical sections were viewed and photographed with a Zeiss LSM 5 PASCAL microscope equipped with epifluorescence optics, using LP560 and LP650 filters and a 40×/1.3 Oil Plan-Neofluar objective.

Electron microscopic immunocytochemistry and morphological analysis. Small blocks of fixed cortex were subjected to freeze substitution as described previously (14). Ultrathin sections were processed for immunogold cytochemistry with the AQP4 antibody (Millipore; 1.5 μg/mL) followed by gold-conjugated secondary antibody (15-nm particles; GAR15 nm; Abcam). Finally, the sections were counterstained and examined in a FEI Tecnai 12 transmission electron microscope.

Detection and quantitation of gold particles. The analyzer was blind to genotype. Digital images were acquired with a commercially available image analysis program (analySIS; Soft Imaging Systems). The program had been modified for acquisition of high-resolution digital images and semiautomatic evaluation of immunogold-labeled cellular volumes and surfaces (membranes). For the present purpose, images of membrane segments were recorded at a nominal magnification of 43,000×, in 2,048 × 2,048 (8-bit) images. All membrane segments that could be identified as belonging to endothelial cells or perivascular endfeet of astrocytes were imaged. Images were taken from five WT, five *Aqp4*$^{-/-}$, three f/f, and four *cAqp4*$^{-/-}$ mice and included the following membrane domains (Fig. 4; *n* = total number of observations for WT, *Aqp4*$^{-/-}$, f/f, and *cAqp4*$^{-/-}$ mice, respectively): astrocyte membrane facing endothelium (72, 91, 66, and 50), endothelial membrane facing astrocyte (76, 90, 54, and 48), endothelial membrane facing pericyte (38, 18, 0, and 0), and luminal endothelial membrane (103, 88, 0, and 0). Membrane segments of interest were drawn in the overlay and assigned a type label. Gold particles in the neighborhood of each membrane curve were detected semiautomatically, and the distance between each particle's center of gravity and its membrane curve were calculated by the program. All images, with associated curves, particles, and measurements, were saved to allow later verification and correction. Further analyses were done in analySIS. Particles localized within 23.5 nm from their membrane curve were included in the automated calculation of the number of particles per unit length of membrane.

The thickness of the basal lamina was measured by manually drawing a line between the abluminal endothelial membrane and the astrocyte endfoot membrane.

Statistical analysis of immunogold data. We used a Poisson mixed model for the gold particle counts (26). This model takes into account the dependency between observations by including three variance terms, one for between animal variation, one for between membrane variation, and one for within membrane variation. For statistical analysis of this model, we used the R function glmer in the lme4 package, which for each membrane gives us estimated differences in linear particle density between genotypes and corresponding *P* values.

Measurement of Brain Water Content. Brain water content was measured with the wet/dry mass method. Subjects were killed via cervical dislocation and brains were immediately dissected out intact. For regional analysis, brains were cut into forebrain/midbrain and brainstem components. The forebrain was additionally divided into hemispheres along the sagittal midline. Each brain sample was manually homogenized with a spatula against the inside of a premassed 10-mL glass vial. The vial was then massed with the brain section, and wet brain sample mass was calculated from the difference. The samples were dried in a Fistreem vacuum oven (Fistreem International) for 24 h at 80 °C and −1,000 mbar. After drying, each vial + brain was again massed. Percent brain water content was calculated as (wet mass − dry mass) × 100/(wet mass). Left and right hemisphere percent water content values were averaged together for each subject. The forebrain values presented represent this average value.

Brain water accumulation after hypoosmotic stress was assessed for each genotype by comparing values for baseline brain water content with brain water content measured on mice decapitated 40 min after i.p. injection of distilled water (150 mL/kg; six f/f and eight *cAqp4*$^{-/-}$ mice). Before injections, mice were anesthetized via an i.p. injection of a mixture of chloral hydrate, magnesium sulfate, and pentobarbital (142, 70, and 32 mg/kg body weight, respectively; Ullevål Sykehusapotek), and kept on a heating pad.

Statistical analyses. Comparison of basal water content among groups was performed via one-way ANOVA, with post hoc comparison via a Bonferroni multiple comparison (Fig. 4*B*). When comparing content in forebrain and brainstem unpaired *t* tests were used (Fig. 4*D*). To compare the brain water content for the genotypes, before and after water injection, we performed a two-way ANOVA. A significant difference between genotypes is equivalent with a significant interaction effect in a two-way ANOVA (Fig. 4*A*). Data are presented as mean ± SE.

Assessment of Blood–Brain Barrier Permeability. Blood–brain barrier permeability to macromolecules was assessed and quantified using a modified version of an established spectrophotometry protocol for the Evans blue albumin dye (27). The control group consisted of seven male f/f mice, whereas the experimental group was composed of five male c*Aqp4*$^{-/-}$mice. All subjects were aged 10–18 wk and weighed 19–34 g.

Evans blue injection. Animals were anesthetized via i.p. injection of a mixture of chloral hydrate, magnesium sulfate, and pentobarbital (142, 70, and 32 mg/kg body weight, respectively; Ullevål Sykehusapotek). Body temperature during anesthesia was continuously maintained via a Harvard Apparatus 101/2 temperature control unit. Evans blue albumin dye (Waldeck; 4% in 0.9% NaCl) was injected (0.004 mL/g) in the retroorbital sinus. Sixty minutes postinjection, subjects were perfused transcardially with 0.9% NaCl (flow rate ∼8 mL/min) for 15 min. The brain was extracted, massed, then transferred to a 15-mL falcon tube containing 3.5 mL formamide (Sigma).

Spectrophotometry. After extraction, brains were left to incubate at 60 °C for 18–24 h. The formamide was extracted and transferred to a 4-mL glass cuvettete, then placed in a PerkinElmer Lambda 1 spectrophotometer, set for 590-nm emission. Absorption (ABS) and percent transmission (% T) were recorded, then used to calculate the concentration of Evans blue present by comparison against a standard curve. Evans blue concentration was normalized to brain mass and formamide volume, yielding a value for micrograms of Evans blue per gram of brain mass. This value was then used for comparison across groups.

Statistical analyses. Comparison among groups was performed via one-way ANOVA, with post hoc comparison via a Bonferroni multiple comparison (Fig. 4*C*). Data are presented as mean ± SE. In all of the statistical analyses, significance was defined at $P < 0.05$. The ANOVAs were performed using the SPSS 7.0 for Windows software package (SPSS).

ACKNOWLEDGMENTS. We thank Mrs. Bjørg Riber, Karen Marie Gujord, Jorunn Knutsen, Carina V. S. Knudsen, and Gaute Nesse for expert technical assistance and Dr. Torgeir Holen for generating constructs for the conditional *Aqp4* knockout mouse line. This work was supported by the Research Council of Norway [NevroNor, and Functional Genomics (FUGE) Grants], Polish–Norwegian Research Fund Grant PNRF-96, and by the Letten Foundation.

1. Bechmann I, Galea I, Perry VH (2007) What is the blood-brain barrier (not)? *Trends Immunol* 28:5–11.
2. Abbott NJ, Rönnbäck L, Hansson E (2006) Astrocyte-endothelial interactions at the blood-brain barrier. *Nat Rev Neurosci* 7:41–53.
3. Reese TS, Karnovsky MJ (1967) Fine structural localization of a blood-brain barrier to exogenous peroxidase. *J Cell Biol* 34:207–217.
4. Manley GT, et al. (2000) Aquaporin-4 deletion in mice reduces brain edema after acute water intoxication and ischemic stroke. *Nat Med* 6:159–163.
5. Nielsen S, et al. (1997) Specialized membrane domains for water transport in glial cells: High-resolution immunogold cytochemistry of aquaporin-4 in rat brain. *J Neurosci* 17:171–180.
6. Amiry-Moghaddam M, Ottersen OP (2003) The molecular basis of water transport in the brain. *Nat Rev Neurosci* 4:991–1001.
7. Verkman AS, Binder DK, Bloch O, Auguste K, Papadopoulos MC (2006) Three distinct roles of aquaporin-4 in brain function revealed by knockout mice. *Biochim Biophys Acta* 1758:1085–1093.
8. Amiry-Moghaddam M, et al. (2004) Alpha-syntrophin deletion removes the perivascular but not endothelial pool of aquaporin-4 at the blood-brain barrier and delays the development of brain edema in an experimental model of acute hyponatremia. *FASEB J* 18:542–544.
9. Kobayashi H, et al. (2001) Aquaporin subtypes in rat cerebral microvessels. *Neurosci Lett* 297:163–166.
10. Sobue K, et al. (1999) Molecular cloning of two bovine aquaporin-4 cDNA isoforms and their expression in brain endothelial cells. *Biochim Biophys Acta* 1489:393–398.
11. Theis M, et al. (2003) Accelerated hippocampal spreading depression and enhanced locomotory activity in mice with astrocyte-directed inactivation of connexin43. *J Neurosci* 23:766–776.
12. Mathiisen TM, Lehre KP, Danbolt NC, Ottersen OP (2010) The perivascular astroglial sheath provides a complete covering of the brain microvessels: An electron microscopic 3D reconstruction. *Glia* 58:1094–1103.
13. Matsubara A, Laake JH, Davanger S, Usami S, Ottersen OP (1996) Organization of AMPA receptor subunits at a glutamate synapse: A quantitative immunogold analysis of hair cell synapses in the rat organ of Corti. *J Neurosci* 16:4457–4467.
14. Haj-Yasein NN, et al. (2011) Evidence that compromised K(+) spatial buffering contributes to the epileptogenic effect of mutations in the human kir4.1 gene (KCNJ10). *Glia* 59:1635–1642.
15. Dolman D, Drndarski S, Abbott NJ, Rattray M (2005) Induction of aquaporin 1 but not aquaporin 4 messenger RNA in rat primary brain microvessel endothelial cells in culture. *J Neurochem* 93:825–833.
16. Eid T, et al. (2005) Loss of perivascular aquaporin 4 may underlie deficient water and K+ homeostasis in the human epileptogenic hippocampus. *Proc Natl Acad Sci USA* 102:1193–1198.
17. Frydenlund DS, et al. (2006) Temporary loss of perivascular aquaporin-4 in neocortex after transient middle cerebral artery occlusion in mice. *Proc Natl Acad Sci USA* 103:13532–13536.
18. Yang J, et al. (2011) Loss of astrocyte polarization in the Tg-ArcSwe mouse model of Alzheimer's disease. *J Alzheimers Dis*, 10.3233/JAD-2011-110725.
19. Agrawal HC, Davis JM, Himwich WA (1968) Developmental changes in mouse brain: Weight, water content and free amino acids. *J Neurochem* 15:917–923.
20. Lehmenkühler A, Syková E, Svoboda J, Zilles K, Nicholson C (1993) Extracellular space parameters in the rat neocortex and subcortical white matter during postnatal development determined by diffusion analysis. *Neuroscience* 55:339–351.
21. Wen H, et al. (1999) Ontogeny of water transport in rat brain: Postnatal expression of the aquaporin-4 water channel. *Eur J Neurosci* 11:935–945.
22. Binder DK, Papadopoulos MC, Haggie PM, Verkman AS (2004) In vivo measurement of brain extracellular space diffusion by cortical surface photobleaching. *J Neurosci* 24:8049–8056.
23. Yao X, Hrabetová S, Nicholson C, Manley GT (2008) Aquaporin-4-deficient mice have increased extracellular space without tortuosity change. *J Neurosci* 28:5460–5464.
24. Saadoun S, et al. (2009) AQP4 gene deletion in mice does not alter blood-brain barrier integrity or brain morphology. *Neuroscience* 161:764–772.
25. Thrane AS, et al. (2011) Critical role of aquaporin-4 (AQP4) in astrocytic Ca2+ signaling events elicited by cerebral edema. *Proc Natl Acad Sci USA* 108:846–851.
26. Albert PS (1999) Longitudinal data analysis (repeated measures) in clinical trials. *Stat Med* 18:1707–1732.
27. Xu Q, Qaum T, Adamis AP (2001) Sensitive blood-retinal barrier breakdown quantitation using Evans blue. *Invest Ophthalmol Vis Sci* 42:789–794.